European Journal of Biophysics
2014; 2(6): 72-80
Published online January 28, 2015 (http://www.sciencepublishinggroup.com/j/ejb)
doi: 10.11648/j.ejb.20140206.11
ISSN: 2329-1745 (Print); ISSN: 2329-1737 (Online)

Kerma and photons absorbed-dose from Ir-192 HDR seeds

Miguel Ángel Chesta[1, 2, *], Ana Lucía Poma[1], Dionisio José Mc Donnell[3]

[1]Facultad de Matemática, Astronomía y Física, Universidad Nacional de Córdoba, Córdoba, Argentina
[2]Instituto de Física Enrique Gaviola, Ifeg, CONICET, Córdoba, Argentina
[3]Departamento de Física Médica, Terapia Radiante Cumbres S.A., Rosario, Argentina

Email address:

chesta@famaf.unc.edu.ar (M. A. Chesta), apoma@famaf.unc.edu.ar (A. L. Poma), josemc@express.com.ar (D. J. Mc Donnell)

To cite this article:

Miguel Ángel Chesta, Ana Lucía Poma, Dionisio José Mc Donnell. Kerma and Photons Absorbed-Dose from Ir-192 HDR Seeds. *European Journal of Biophysics.* Vol. 2, No. 6, 2014, pp. 72-80. doi: 10.11648/j.ejb.20140206.11

Abstract: Precise calculations of absorbed dose (AD) are a difficult task involving physical phenomena such as emission, transport, and absorption of radiation. We used the Monte Carlo method to calculate Kerma as well as AD in water imparted by two different *Ir-192* HDR brachytherapy seeds (*Flexisource* and *microSelectron-v2*) taking into account the AAPM TG-43 formalism and AAPM & ESTRO most recent reports recommendations. The aim of this work is to evaluate when can Kerma be used as a measurement of AD for this type of seeds. Thus, we analyse the behaviour of both quantities in whole space, putting special emphasis near the source surface. We carried out calculations using microvoxels to obtain high spatial resolution of data close to the source. We observed differences of up to *6 %* between AD and Kerma within 1 mm around the seed, and less than *1 %* in any other region of the phantom. This allows us to analyse build-up region for *Ir-192* HDR brachytherapy seeds. As it will be further discussed in this paper, our results can be explained in terms of partial electronic equilibrium reached on different regions of the phantom. Both seeds showed common overall behaviour, providing generality to the conclusions drawn. The complete bearing of the radial dose function (defined in the TG43 formalism) as it traverses the surface of the seed is reported. Whenever comparisons are possible, our results are in agreement with those reported by other authors. Tables of radial dose function, including new data computed from AD rate (instead of Kerma rate), are presented.

Keywords: Photons Absorbed Dose, Kerma, HDR-Brachytherapy, Seed, Ir-192

1. Introduction

In HDR-brachytherapy treatment, the radioisotope *Ir-192* is used due to its specific-activity and the characteristics of its photon-spectrum in a sealed source form. For use in treatment, these sources are manufactured in miniaturized size of approximately cylindrical shape (about *1 mm* diameter by several millimetres long, see Fig. 1) and they are known as seeds. The seeds may vary slightly in design depending on the manufacturer [1]. All HDR-brachytherapy seeds have a steel-shielding that covers their *iridium* core. This shielding provides rigidity to seeds, being designed to stop beta-particles from radioactive decay while allowing the outward of photons flux.

During treatment, the seed is inserted into the patient using an applicator. Radiation emitted from the source (*i.e.* primary photons) interacts with the surrounding environment (human tissue) setting in motion secondary electrons. Along their path, the kinetic energy of the secondary electrons is absorbed by the medium. By means of this process, radiation-dose is absorbed by the tissues.

In regions of space where electronic equilibrium is attained, AD (absorbed dose) from primary-photons can be inferred from knowledge of Kerma (kinetic energy released per unit mass). In contrast, near seed surface there is a build-up region where electronic equilibrium is not achieved and marked differences between Kerma and AD are expected. Other authors [4-6] have attempted to characterize this build-up region in the past. Although, as it will be further discussed in this paper, calculations achieved by them are based in models of simplified situations. We have not found precise reports of direct-computation of AD over the entire region around the seeds. The use of Kerma as a measure of AD from photons remains a current topic of discussion.

In addition, precise knowledge of the AD distribution in water is required in order to plan the treatment. The Monte Carlo (MC) simulation method showed being an appropriate tool for calculating AD distribution in a medium around the seed [7]. The MC implementation to this problem requires following a set of well-established protocols [1, 8-9]. Calculating AD is more complex than Kerma computation and consequently, it requires increased computational time.

Thus, it is important to determine precisely in which situations AD can be inferred from Kerma computation, this being one of the goals of this work.

It is important to state that in the past, many authors have applied the MC method to model HDR-brachytherapy seeds with several degrees of approximation and to calculate Kerma in a water-phantom: *microSelectron-v2* [3, 10-11], *microSelectron-v2r* [12] (slightly different from *v2* seed) and *Flexisource* [2, 11]. According to the literature on this subject, to calculate AD even closer to the seeds, authors frequently have resorted to data extrapolation [1].

2. Materials and Methods

In this work we used the MC PENELOPE *v2008* code [13-14] together with the clonEasy simulation package available at http://inte.upc.edu/downloads [15]. Two available commercial *Ir-192* HDR-brachytherapy seeds have been modelled: *Flexisource* and *microSelectron-v2*. Radiation transport in water has been simulated following recommendations given by AAPM in TG43 formalism [8] and its update: TG43U1 [9] and new AAPM and ESTRO report [1]. The photons interactions considered in the PENELOPE MC code are: Rayleigh dispersion, photoelectric absorption, Compton dispersion and pair production. The photoelectric absorption cross-sections used by PENELOPE are interpolated from the LLNL evaluated photon data library [16] (EPDL). Differential cross-sections (DCS) per unit solid angle for Rayleigh dispersion are calculated using non-relativistic perturbation theory with atomic form factors obtained from EPDL library [16]. Compton dispersion is described according to the relativistic impulse approximation [17] where the Doppler broadening effect is taken into account. For pair-production a semi-empirical model based in Bethe-Heitler DCS equation is used [18]. As regards electrons, PENELOPE implements a combined detailed-simulation of hard events and condensed-simulation of soft events in a mixed scheme [19-21]. Concerning electrons and positrons, elastic scattering cross-sections are computed using interpolation of numerical DCS from the ELSEPA database. The simulation of inelastic collision of electrons and positrons is performed according to Bethe and Fano DCS equation, and on the basis of an atomic generalized oscillator model. The DCS for *bremsstrahlung* emission is based on the Seltzer and Berger original database [19, 20].

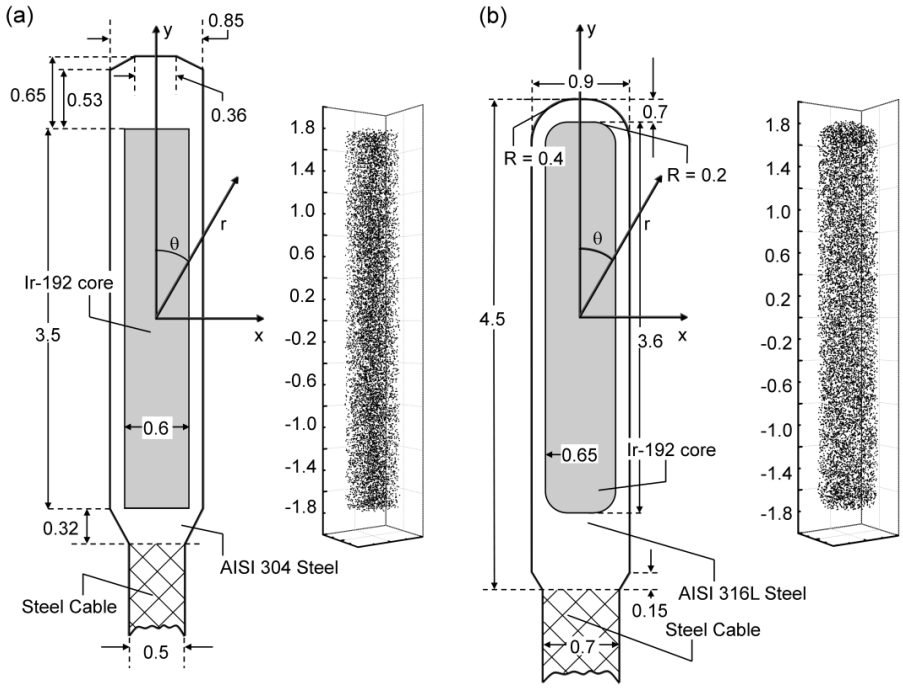

Figure 1. *Modelled HDR brachytherapy Ir-192 seeds: (a) Flexisource and (b) microSelectron-v2. Geometry dimensions (in mm) and composition of commercial seeds were taken from literature (Flexisource [2], microSelectron-v2 [3]). Simulated homogeneous nuclear distribution for each of the seeds modelled in this work is also included (in low statistic, only for visualizing purposes).*

Both, seeds composition and geometry have been taken from the literature: Daskalov *et al* [3] for *microSelectron-v2* seed and Granero *et al* [2] for *Flexisource* seed. Active core was modelled by a homogeneous iridium atoms distribution taking into account precise cylindrical geometry of each one of the seeds (see Fig. 1). The seeds were modelled including the stainless steel capsule and flexible cable for remote positioning. The *3-D* space in which all physical processes were simulated consisted of a spherical water phantom (*40 cm* radius) with the seeds positioned at its centre. Discretization of the region where Kerma and AD are calculated is achieved into cubic voxels with varying edge-lengths: *0.01 mm*, *0.1 mm* or *1 mm* (increasing with seeds surface distance). This high spatial resolution compromises the minimum number of simulated histories necessary to achieve statistically representative data. In addition, studying dose high spatial-gradient without introducing additional error requires considering voxel dimensions appropriated to

this end. Otherwise, calculation of the near-seed dose could be over- or under-estimated in calculations. Table I displays data from the literature [2-3] that has been used in this work to model seeds and phantoms.

Table I. *Main geometry dimensions of phantoms and seeds, and densities and composition by weight of each material simulated in this work: (a) Flexisource [2] and (b) microSelectron-v2 [3].*

	Flexisource	***microSelectron-v2***
Active Core	Ir-192	
Length (mm)	3.5	3.6
Diameter (mm)	0.6	0.65
Iridium (%)	100	
Density (g/cm^3)	22.42	
Steel capsule and cable	AISI 304	AISI 316L
Capsule diameter (mm)	0.85	0.90
Cable length (mm)	5.0	2.0
Carbon (%)	0.08	0.03
Nitrogen (%)	0.10	
Silicon (%)	0.75	
Chromium (%)	19.00	17.00
Manganese (%)	2.00	
Iron (%)	68.75	65.55
Nickel (%)	9.25	12.00
Molybdenum (%)	--	2.50
Steel capsule density (g/cm^3)	8.00	8.03
Steel cable density (g/cm^3)	6.10	4.81
Water phantom		
Sphere diameter (cm)	80	
Hydrogen (%)	11.1	
Oxygen (%)	88.9	
Density (g/cm^3)	0.998	
Air phantom (Humidity 0%)		
Sphere diameter (m)	5.5	
Hydrogen (%)	0.0732	
Oxygen (%)	23.6077	
Nitrogen (%)	75.0325	
Carbon (%)	0.0123	
Argon (%)	1.2743	
Density (g/cm^3)	0.00120	

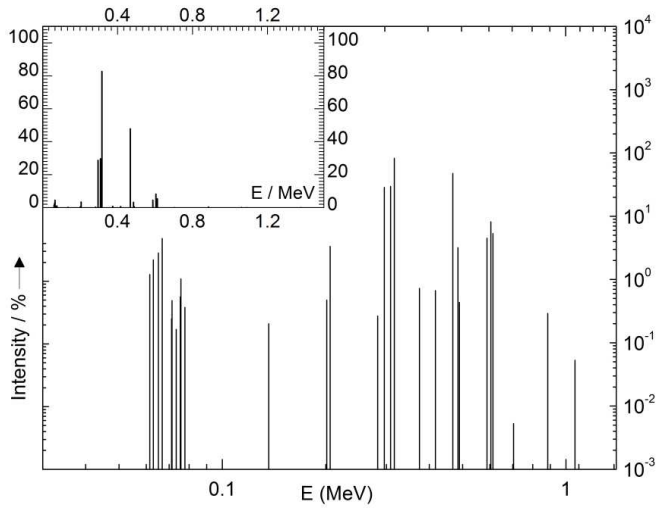

Figure 2. *Energy spectrum corresponding to photons emitted by Ir-192 in 100 decayment events to Os*-192 (EC, 5 %) and Pt*-192 (β^-, 95 %) isobars in nuclear and atomic excited states. In embedded window, photon groups of greater intensity are appreciated.*

In order to use the TG-43 formalism and compare Kerma with photons-AD, we have considered only *X*- and γ-rays as primary radiation [24], without including β particles, Auger or CE (conversion electrons, see Fig. 2). Such particles are largely blocked by the steel-shielding that constitutes the capsule of the seeds (see Fig. 1). Besides this, the main goal of this work is to evaluate validity of Kerma as a measure of water AD from photons. In AD computation, simulation process of each history ends when average kinetic energy of all set-in-motion electrons ensure this energy is deposited in a voxel, and represents cut-off energy. We set cut-off energy of 10^3 *eV* in this work simulation. This cut-off energy value ensures that the linear dimensions of the voxel are greater by an order of magnitude than the mean-range of electrons of kinetic energy equal to cut-off energy. Secondary radiation is also taken into account for AD computation. This secondary radiation is mainly produced during the slowing down of secondary or ternary particles (*i.e.* electrons, positrons and delta rays) and its intensity might be great in certain conditions [25-26].

The empiric-analytical protocol TG43 [1, 8-9] is a procedure through which it is possible to determine AD rate in water around the seed. By this formalism and taking into consideration the revolution symmetry of the seed absorbed dose rate $\dot{D}$ is defined in spherical coordinates by the expression:

$$\dot{D}(r,\theta) = S_K \Lambda \frac{G_L(r,\theta)}{G_L(r_0,\theta_0)} g_L(r) F_L(r,\theta) \tag{1}$$

where S_K is air Kerma strength at *1 m* distance of the source centre. The dose rate constant Λ represents the absorbed dose rate at reference distance r_0 (with r_0 = *1 cm*) on the mid transverse plane ($\theta = \theta_0$ with $\theta_0 = \pi/2$) related to S_K. $G_L(r, \theta)$ is the geometry function in the line source approximation:

$$G_L(r,\theta) = \begin{cases} \dfrac{\beta(r,\theta)}{rL\sin(\theta)} & if\ \theta \neq 0 \\ \dfrac{1}{r^2 - \left(\dfrac{L}{2}\right)^2} & if\ \theta = 0 \end{cases} \tag{2}$$

where β is the angle, in radians, subtended by the tips of the hypothetical line source with respect to the calculation point, $P(r, \theta)$. $g_L(r)$ is the radial dose function given by:

$$g_L(r) = \frac{G_L(r_0,\theta_0)}{G_L(r,\theta_0)} \frac{\dot{D}(r,\theta_0)}{\dot{D}(r_0,\theta_0)} = \frac{r}{r_0} \frac{\beta_0(r_0)}{\beta_0(r)} \frac{\dot{D}_0(r)}{\dot{D}_0(r_0)} \tag{3}$$

where $\beta_0(r) = \beta(r, \theta_0)$ and $\dot{D}_0(r) = \dot{D}(r,\theta_0)$. Eq. (3) takes into account the radial dependence of absorption and dispersion of photons in water along the transverse distance from the source. The quantity $F(r, \theta)$ is the anisotropy function defined by:

$$F(r,\theta) = \frac{G_L(r,\theta_0)}{G_L(r,\theta)} \frac{\dot{D}(r,\theta)}{\dot{D}(r,\theta_0)} = \frac{\beta_0(r)}{\beta(r,\theta)} \frac{\dot{D}(r,\theta)}{\dot{D}_0(r)} sen(\theta) \tag{4}$$

Thus, based on eq. (1) and tabulated data of Λ, g_L and F for a given seed, it is possible to know $\dot{D}$ in the whole space (defined by the phantom). Moreover, it should be noted from eq. (3) that the dependence of $\dot{D}$ with the r-variable directly influences the function g_L which is proportional to $\dot{D}_0(r)$ multiplied by the geometry factor $r/\beta_0(r)$. Conversely, a poor dependence of $F(r, \theta)$ onto the radial behaviour of $\dot{D}$ is expected. This statement is due to the observed proportionality between $F(r, \theta)$ and dose rate profile $\dot{D}(r,\theta)/\dot{D}_0(r)$ in eq. (4).

3. Results and Discussion

In each simulation, the total number of histories simulated was 10^{11} and the uncertainties achieved were Type A (k=1) less than *0.1 %* for distances $r \leq 5\,cm$ and less than *0.2 %* for distances $r \leq 10\,cm$ as recommended in AAPM and ESTRO new report [1]. The results of the simulations for both seeds are presented as Kerma rate $\dot{K}_0(r)/\dot{K}_0(r_0)$ and photons-AD rate profiles $\dot{D}_0(r)/\dot{D}_0(r_0)$ (Fig. 3) and over the 3 material media (iridium, steel and water). From the high spatial resolution set out by the simulation, we are able to precisely compute $\dot{K}$ and $\dot{D}$ on both sides of the steel-water interface (as well as the iridium-steel interface). AD must change continuously when crossing any interface and a detailed analysis of the steel-water interface is particularly important because it allows us to accurately know the behaviour of AD on seeds surface. AD continuity in the interface is consequence of the secondary electrons trajectory not being cut at the frontier (secondary electrons deposit energy on interface both sides). Differing from AD, Kerma presents discontinuities on interfaces since photon attenuation in each material medium is different. Besides, computing Kerma considers secondary electrons deposit kinetic energy at the same place they are set in motion.

Charts embedded in figs. 3a (*Flexisource*) and 3b (*microSelectron-v2*) show this different behaviour between Kerma and photons-AD profiles. We observed that next to the steel interface in water phantom ($r \leq 0.2\,cm$), photons-AD profile oscillates around Kerma profile for both seeds. Photons-AD profile initially shows depression with respect to Kerma profile very-close to seed surface, then both profiles become equal (in $r \cong 0.05\,mm$ for both seeds) followed by an inverse behaviour in which photons-AD profile exceeds Kerma profile forming a peak. This peak in photons-AD profile over Kerma profile on seeds vicinity might be explained from a reinforcement of the secondary electrons density in the aqueous side of the steel-water interface. Water has lower effective atomic number and lower density than those of steel and this causes photons-AD profile to be greater than Kerma profile in the region. In this area there are backscattered electrons from the steel (capsule) to the aqueous medium (phantom). No electronic equilibrium is established in the region nearest the seeds ($r < 2\,mm$).

The differences that we found between Kerma rate and photons-AD rate profiles for both seeds are up to *6.4 %* (around $r = 0.07\,mm$, see embedded charts on Figs. 3a y 3b). Further from seeds surface the differences between Kerma and photons-AD profiles remained limited within *1 %*, with Kerma profile below photons-AD profile as a consequence of the attenuation of the primary photons in water [27].

The differences in observed behaviour between $\dot{D}$ and $\dot{K}$ profiles can be explained by the lack of electronic equilibrium near seeds surface, corresponding to the build-up region. This process dominates up to a distance that is equivalent to the range of the secondary electrons of higher energy (*i.e.* approximately *2 mm*, for photo-electrons of *0.6 MeV*). According to the energy spectrum that these seeds emit (Fig. 2), the most energetic photons with appreciable intensity (see embedded chart in Fig. 2) correspond to energy of *0.6 MeV*. These photons are capable of producing secondary electrons with kinetic energy close to *0.6 MeV*. Once this "equilibrium thickness" is surpassed, it is observed that both quantities (photons-AD and Kerma profiles) diminish parallel to each other (see Fig. 3) with photons-AD above Kerma. For both seeds, the difference between these two quantities (photons-AD and Kerma profiles) is less than *1%* and this behaviour is observable for both seeds (as an example, see Fig. 3c for *Flexisource* seed). In this region, farther from seeds surface the small differences observed between Kerma and photons-AD profiles indicate that the primary-photons attenuation is a process that could be compensated partially by another one, originating in the secondary-electrons *bremsstrahlung*-losses. Primary-photons attenuation helps photons-AD to be greater than Kerma, photons-AD at one point would equal Kerma at another point at which primary-photons density is greater. On the other hand, radiation losses diminish photons-AD but not Kerma. Hence, primary- photons attenuation process would be barely more important than secondary-particles radiation, making photons-AD profile to prevail over Kerma profile, although just in a small amount.

As it has been mentioned before (see introduction section) several authors have studied build-up region in the past for HDR-brachytherapy seeds. These computations were based on simplified seeds modelling, either in seed design and/or in the energy spectrum emitted by it. Ballester *et al* [4] calculated AD in water from spherical *Ir-192* seeds in a steel capsule. These spheres have an active core diameter and capsule thickness comparable to transversal seed dimensions. They found an oscillating behaviour between photons-AD and Kerma similar to the one found in this work, where no approximations have been made. Luxton and Joszef [6] evaluated AD in water by mono-energetic photon-emitting point sources ranging from *10 keV* to *2 MeV*. They found build-up regions of *1 mm* for *500 keV* sources and *2 mm* for *800 keV* sources. This result is also consistent with the one achieved for the seeds simulated in this work without simplifications, either in seeds geometry or in seed photon-emitting spectrum.

Table II displays the results achieved in this work for both seeds Kerma values relative to photons-AD. Results achieved in this work for microSelectron-v2 seed are compared to those achieved by other authors in the past [4, 11, 28]. On the

right of each column that corresponds to quotient $\dot{K}(r)/\dot{D}(r)$ values achieved by other authors, another column with percentage differences δ % between our results and those from these authors is added. From table II, general agreement among different authors results may be observed. The differences found between this work results and those of other authors are mostly less than or equal *2 %*. For *Flexisource* seed, it has not been possible to compare our results of kerma rate to dose rate values because of the lack of other authors results of photons-AD and Kerma in the near-seed region.

From eq. (3) and $\dot{K}$ and $\dot{D}$ profiles we computed radial dose functions from Kerma ($g_{L,K}(r)$) and from photons- AD ($g_{L,D}(r)$) for both seeds (see Fig. 4). For both seeds, it is observed that $g_{L,D}(r)$ clearly deviates from $g_{L,K}(r)$ up to around *2 mm* distance. This distance corresponds to the equilibrium thickness (see embedded charts in Figs. 4a and 4b). The differences between $g_{L,K}(r)$ and $g_{L,D}(r)$ in this region, up to *6.4 %* are a consequence of the same relative differences on photons-AD rate and Kerma rate profiles. The function obtained from our data continues very close to the one obtained from photons-AD rate profile although $g_{L,D}(r)$ values stay just above, this difference being less than or equal *1 %*. Results achieved in this work for *g(r)* are consistent with the ones calculated in the past by Granero *et al* [2], Daskalov *et al* [3] corrected to full scattering conditions [1, 29] and Taylor and Rogers [11]. Table III in the appendix contains values achieved in this work for dose rate profile $\dot{D}_0(r)/\dot{D}_0(r_0)$ and $g_{L,D}(r)$ photons-AD radial dose function and are presented with spatial resolution of *0.05 mm* up to *5 mm*.

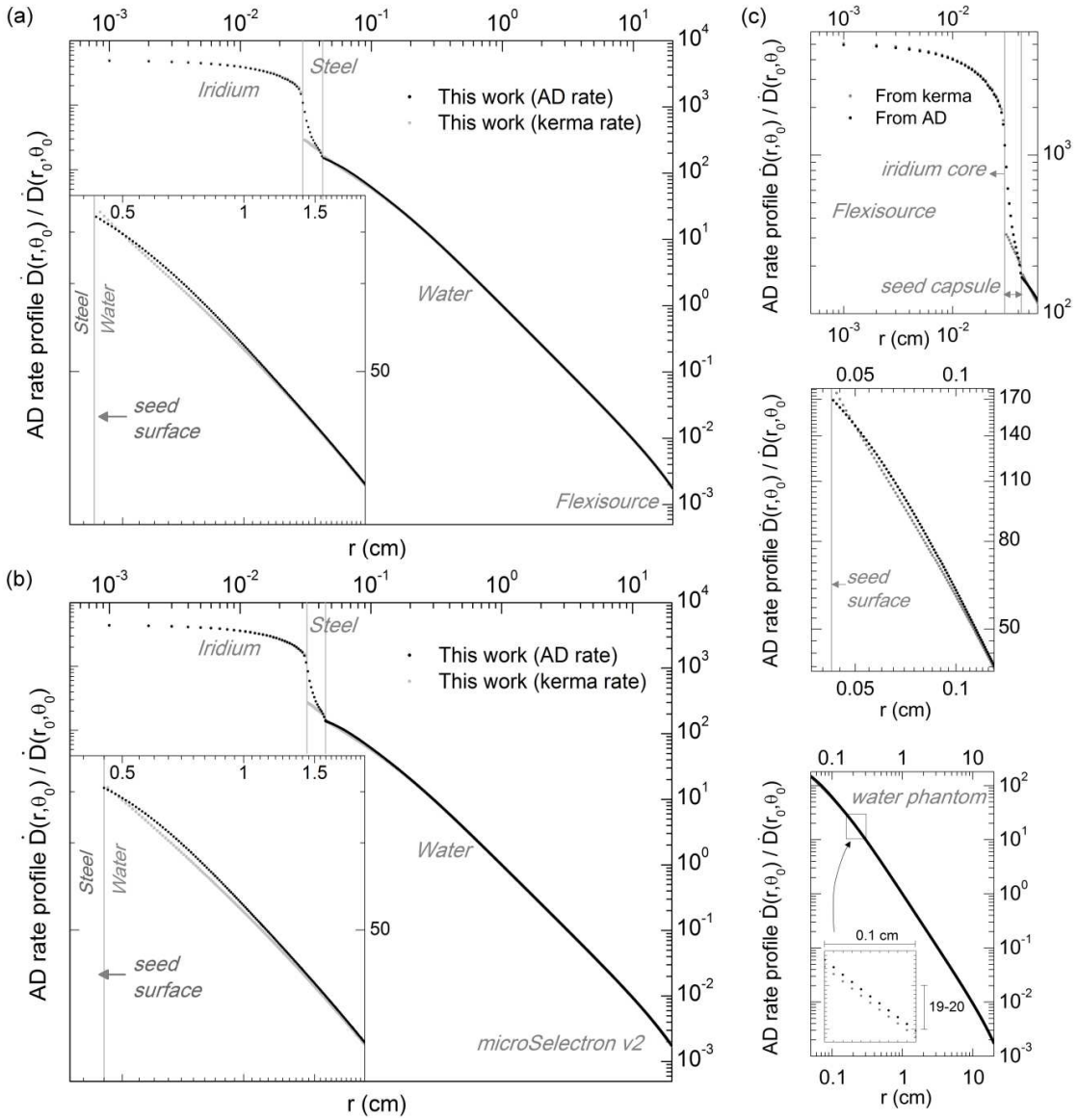

Figure 3. *Dose rate profiles for $\theta = \theta_0$ calculated from photons-AD rate (black scatter) and Kerma rate (gray scatter): (a) Flexisource results from this work and (b) microSelectron-v2 results from this work. Embedded window chart shows amplification of photons-AD and Kerma rate profiles near steel-water interface in figures (a) and (b). In (c), amplification shows photons-AD rate and Kerma rate profiles in three different segments: inside the seed (iridium core and steel capsule), near seed capsule and water phantom for Flexisource seed.*

Table II. *Kerma values related to photons-AD achieved in this work are compared to those obtained by other authors in the past: Wang and Li [27], Taylor and Rogers [10], Ballester et al [4] for microSelectron-v2 seed. On the right of each column of results from other authors, another δ% percentage difference column (between this work and other author values) is added. Only this work results are presented for Flexisource seed because of the lack of Kerma and photons-AD rate near-source results from other authors.*

r (mm)	$\dot{K}(r)/\dot{D}(r)$							
	Flexisource	***microSelectron v2***						
	This work	**Wang and Li 2002**	**δ (%)**	**Taylor and Rogers 2008**	**δ (%)**	**Ballester *et al* 2009**	**δ (%)**	**This work**
0.44	1.059	--	--	--	--	--	--	--
0.45	1.045	--	--	--	--	--	--	--
0.46	1.033	--	--	--	--	--	--	1.018
0.47	1.022	--	--	--	--	--	--	1.008
0.48	1.013	--	--	--	--	--	--	0.999
0.49	1.004	--	--	--	--	--	--	0.992
0.50	0.997	1.035	5.2	--	--	0.997	1.3	0.984
0.55	0.970	--	--	--	--			0.958
0.60	0.957	0.961	2.0	0.958	1.7	0.973	3.3	0.942
0.65	0.951	--	--	--	--	--	--	0.934
0.70	0.949	0.942	1.2	0.941	1.1	0.941	1.1	0.931
0.75	0.949	--	--	--	--	--	--	0.932
0.80	0.952	0.940	0.6	0.943	1.0	0.935	0.1	0.934
0.85	0.955	--	--	--	--	--	--	0.938
0.90	0.959	0.946	0.4	0.952	1.1	0.940	0.2	0.942
0.95	0.964	--	--	--	--	--	--	0.946
1.00	0.968	0.959	0.9	0.960	1.1	0.951	0.1	0.950
1.10	0.976	--	--			0.961	0.3	0.958
1.20	0.982	--	--	0.978	1.6	0.972	0.9	0.963
1.30	0.986	--	--			0.978	1.0	0.968
1.40	0.989	--	--	0.986	1.5	0.982	1.1	0.971
1.50	0.990	--	--			0.986	1.1	0.975
1.60	0.991	--	--	0.990	1.3	0.988	0.9	0.977
1.70	0.992	--	--			0.992	1.2	0.980
1.80	0.991	--	--	0.995	1.3	0.995	1.3	0.982
1.90	0.992	--	--			0.995	1.1	0.984
2.00	0.994	0.991	0.5	0.999	1.3	0.994	0.8	0.986

4. Conclusions

For this work we have selected two of the most commonly used seeds, which remain valid today in many medical centres for HDR-brachytherapy treatments. The selected seeds (*Flexisource* and *microSelectron-v2*) come from different manufacturers, giving greater generality to the conclusions achieved in this work.

On the other hand it should also be noted that seeds modelling and cross sections used in our simulations were the same for both: Kerma rate and photons-AD rate calculations. Thus the observed differences in behaviour between Kerma and photons-AD profiles are attributed exclusively to partial loss of electronic equilibrium in different regions of the space surrounding the seeds.

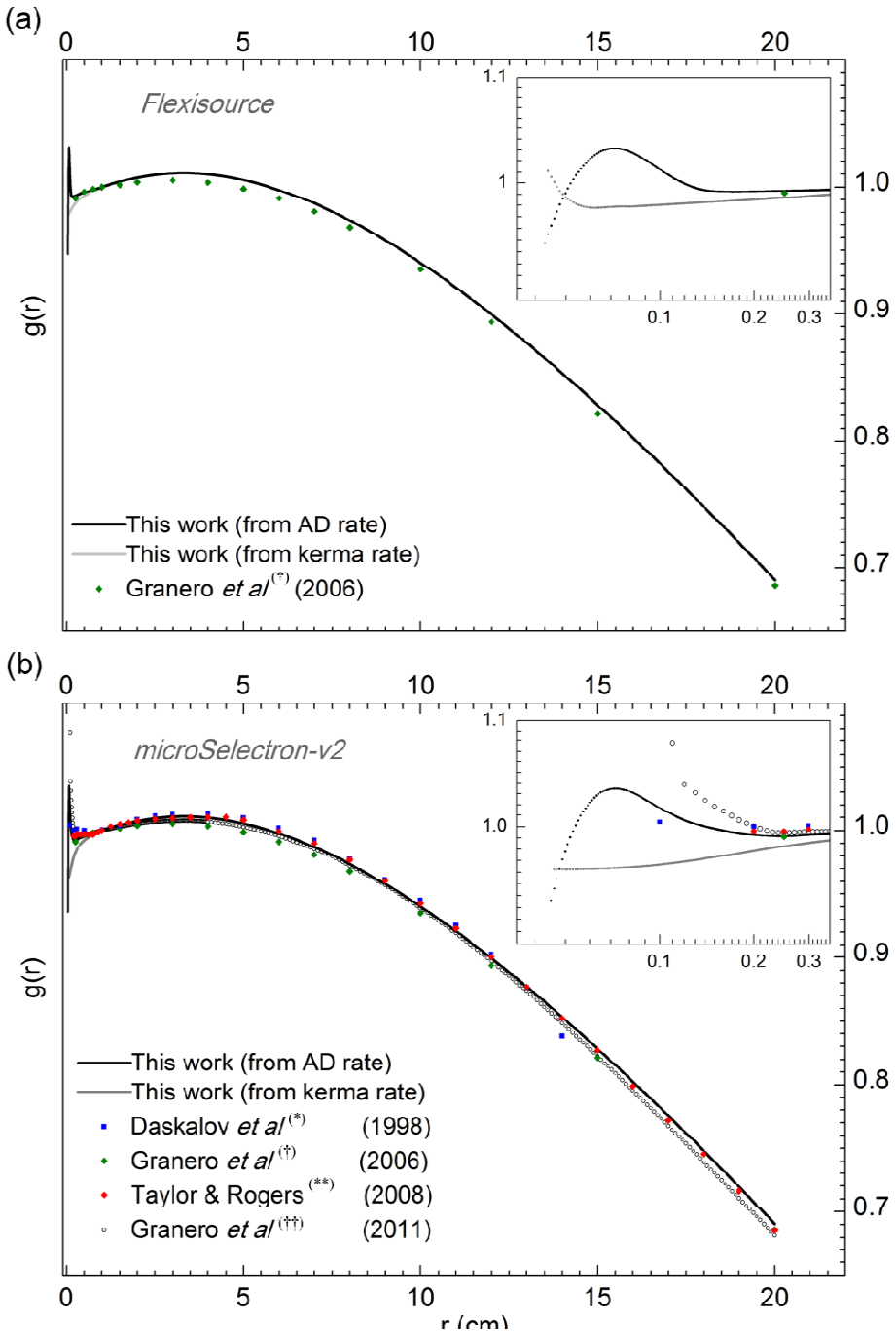

Figure 4. *Radial dose function calculated from photons-AD rate $g_{LD}(r)$ (black line) and Kerma rate $g_{LK}(r)$ (gray line) are presented. In (a), this work Flexisource data is compared to the ones obtained by Granero et al [2] in green diamonds. In (b), this work microSelecetron-v2 data is compared to those obtained by Daskalov et al [3] in blue squares (*), Granero et al [2] in green diamonds (†), Taylor and Rogers [11] in red diamonds (**), and Granero et al [12] in black line and white filled circles (††). (*) Achieved from Kerma rate profile, and corrected to full scattering conditions [1, 29]. (†) From Kerma rate profile. (**) From AD rate profile. (††) Mixed form AD rate and Kerma rate profiles, and for microSelectron-v2r seed. Granero et al [12] AD profile dose rate function includes and electrons emitted from source.*

Phantom discretization into small voxels (see Section 2) was due to the need for greater spatial resolution than that achieved in the past according to the literature of the subject, mainly in the area of high spatial-gradient close to the seed. We found, as expected, a continuous behaviour of photons-AD across the steel-water interface opposite to Kerma which showed a discontinuity in the same interface. By using high spatial resolution and the continuity of AD through the interface, it was possible to calculate the precise value of photons-AD on seeds surface. Analysing these results on the three material media (*iridium*, steel and water) and particularly in the steel-water interface, we found that we were able to calculate AD with precision in the build-up region. Whenever comparisons are possible, our results are in agreement with those reported by other authors.

Quantities g_L, F and Λ completely characterize delivered

dose in water from *Iridium*-192 seeds that are commonly used in HDR-brachytherapy, since they allow obtaining AD in water in the space surrounding the seeds. From those quantities (by its definition in TG43 formalism), function $g_L(r)$ can be seen to be directly affected by radial behaviour of absorbed dose profile.

Acknowledgment

Special acknowledgment must be expressed to Secyt-UNC for its financial support in this paper.

Appendix

Table III. *Both seeds photons-AD rate profile D0(r)/D0(r0) (in a) and radial dose function gL,D(r) calculated from photons-AD rate profile (in b) achieved in this work are presented in r-steps of 0.05 mm up to a distance of 5 mm. Each column contains data for both simulated seeds: Flexisource (on the left) and microSelectron-v2 (on the right).*

a)

$\dot{D}_0(r)/\dot{D}_0(r_0)$										
r (mm)	**0**		**1**		**2**		**3**		**4**	
.00	--- ---		60.748	61.457	20.423	20.595	10.041	10.097	5.9015	5.9202
.05	--- ---		56.522	57.122	19.587	19.752	9.7445	9.7975	5.7651	5.7830
.10	--- ---		52.737	53.241	18.800	18.959	9.4610	9.5106	5.6333	5.6504
.15	--- ---		49.332	49.755	18.059	18.211	9.1893	9.2359	5.5059	5.5223
.20	--- ---		46.257	46.615	17.361	17.506	8.9290	8.9727	5.3828	5.3984
.25	--- ---		43.470	43.777	16.701	16.840	8.6792	8.7203	5.2637	5.2786
.30	--- ---		40.934	41.202	16.077	16.210	8.4396	8.4783	5.1484	5.1627
.35	--- ---		38.616	38.858	15.486	15.614	8.2096	8.2460	5.0368	5.0505
.40	--- ---		36.491	36.715	14.928	15.049	7.9887	8.0230	4.9288	4.9419
.45	154.82	162.78	34.536	34.751	14.399	14.514	7.7764	7.8087	4.8241	4.8368
.50	142.75	147.84	32.734	32.943	13.897	14.006	7.5723	7.6027	4.7228	4.7349
.55	130.79	134.24	31.068	31.273	13.421	13.523	7.3759	7.4047	4.6245	4.6361
.60	119.48	121.99	29.523	29.728	12.968	13.065	7.1869	7.2141	4.5293	4.5404
.65	109.04	111.02	28.090	28.292	12.538	12.629	7.0049	7.0307	4.4369	4.4476
.70	99.575	101.23	26.757	26.952	12.129	12.214	6.8295	6.8541	4.3473	4.3575
.75	91.086	92.512	25.515	25.709	11.739	11.818	6.6605	6.6840	4.2603	4.2702
.80	83.512	84.764	24.356	24.548	11.367	11.441	6.4976	6.5200	4.1759	4.1854
.85	76.778	77.878	23.274	23.462	11.012	11.082	6.3405	6.3619	4.0940	4.1031
.90	70.797	71.758	22.261	22.445	10.674	10.739	6.1593	6.1796	4.0144	4.0231
.95	65.482	66.311	21.313	21.491	10.350	10.411	6.0427	6.0622	3.9371	3.9455

b)

$g_{L,D}(r)$										
r (mm)	**0**		**1**		**2**		**3**		**4**	
.00	--- ---		1.0124	1.0171	0.9927	0.9927	0.9938	0.9927	0.9948	0.9942
.05	--- ---		1.0085	1.0136	0.9928	0.9924	0.9938	0.9928	0.9948	0.9943
.10	--- ---		1.0049	1.0106	0.9928	0.9922	0.9939	0.9929	0.9949	0.9943
.15	--- ---		1.0019	1.0081	0.9929	0.9921	0.9939	0.9930	0.9949	0.9944
.20	--- ---		0.9994	1.0059	0.9929	0.9919	0.9940	0.9931	0.9950	0.9944
.25	--- ---		0.9973	1.0041	0.9930	0.9918	0.9940	0.9932	0.9950	0.9945
.30	--- ---		0.9958	1.0025	0.9930	0.9917	0.9941	0.9933	0.9951	0.9945
.35	--- ---		0.9946	1.0012	0.9931	0.9916	0.9941	0.9934	0.9951	0.9946
.40	--- ---		0.9938	1.0001	0.9932	0.9915	0.9942	0.9935	0.9952	0.9946
.45	0.9621	0.9358	0.9933	0.9991	0.9932	0.9915	0.9942	0.9936	0.9952	0.9947
.50	0.9908	0.9779	0.9929	0.9982	0.9933	0.9915	0.9943	0.9937	0.9953	0.9947
.55	1.0102	1.0054	0.9927	0.9973	0.9933	0.9916	0.9943	0.9937	0.9953	0.9948
.60	1.0222	1.0221	0.9926	0.9966	0.9934	0.9916	0.9944	0.9938	0.9954	0.9948
.65	1.0288	1.0310	0.9926	0.9959	0.9934	0.9917	0.9944	0.9939	0.9954	0.9949
.70	1.0314	1.0345	0.9924	0.9952	0.9935	0.9919	0.9945	0.9939	0.9954	0.9949
.75	1.0310	1.0346	0.9924	0.9946	0.9935	0.9920	0.9945	0.9940	0.9955	0.9950
.80	1.0287	1.0323	0.9925	0.9941	0.9936	0.9921	0.9946	0.9940	0.9955	0.9950
.85	1.0252	1.0289	0.9925	0.9937	0.9936	0.9922	0.9946	0.9941	0.9956	0.9951
.90	1.0211	1.0249	0.9926	0.9933	0.9937	0.9924	0.9947	0.9941	0.9956	0.9951
.95	1.0167	1.0209	0.9927	0.9929	0.9937	0.9925	0.9947	0.9942	0.9957	0.9952

References

[1] Pérez-Calatayud J, Ballester F, Das RK, DeWerd LA, Ibbott GS, Meigooni AS, Ouhib Z, Rivard MJ, Sloboda RS and Williamson JF (2012) Dose calculation for photon-emitting brachytherapy sources with average energy higher than 50keV: Report of the AAPM and ESTROMed. Phys. 39(5) 2904-29.

[2] Granero D, Pérez-Calatayud J, Casal E, Ballester F and Venselaar J (2006) A dosimetric study on the Ir-192 high dose rate FlexisourceMed. Phys. 33(12) 4578-82.

[3] Daskalov GM, Georgi M, Löffler E, Williamson JF and Jeffrey F (1998) Monte Carlo-aided dosimetry of a new high dose-rate brachytherapy source Med. Phys. 25(11) 2200-8.

[4] Ballester F, Granero D, Pérez-Calatayud J, Melhus CS and Rivard MJ (2009) Evaluation of high-energy brachytherapy source electronic disequilibriumand dose from emitted electronsMed. Phys. 36(9) 4250-5.

[5] Chen Z and Nath R (2001) Dose rate constant and energy spectrum of interstitial brachytherapy sourcesMed. Phys. 28(1) 86-96.

[6] Luxton G and Jozsef G (1999) Radial dose distribution, dose to water and dose rate constant for mono-energetic photon point sources from 10 keV to 2 MeV: EGS4 Monte Carlo model calculation Med. Phys. 26(12) 2531-8.

[7] Kumar S, Deshpande DD and Nahum AE (2015) Monte-Carlo-derived insights into dose–kerma–collision kerma inter-relationships for 50 keV–25 MeV photon beams in water, aluminium and copper Phys. Med. Biol. 60 501-19.

[8] Nath R, Anderson LL, Luxton G, Weaver KA, Williamson JF and Meigioni AS (1995) Dosimetry of interstitial brachytherapy sources: Recommendations of the AAPM Radiation Therapy Committee Task Group No. 43 Med. Phys. 22 209-234.

[9] Rivard M, Coursey B, DeWerd L, Hanson W, SaifulHuq M, Ibbott G, Mitch M, Nath R and Williamson J (2004) Update of AAPM Task Group No. 43 Report: A revised AAPM protocol for brachytherapy dose calculations Med. Phys. 31 633–74.

[10] Papagiannis P, Angelopoulos A, Pantelis E, Sakelliou L, Baltas D, Karaiskos P, Sandilos P and Vlachos L (2002) Dosimetry comparison of 192 Ir sources Med. Phys. 29(10) 2239–46.

[11] Taylor RE and Rogers DWO (2008) EGSnrc Monte Carlo calculated dosimetry parameters for 192-Ir and 169-Yb brachytherapy sources Med. Phys. 35(11) 4933–44.

[12] Granero D, Vijande J, Ballester F and Rivard M (2011) Dosimetry revisited for the HDR mHDR-v2 Med. Phys. 38(1) 487–94.

[13] Salvat F, Fernandez-Varea J M, Acosta E and Sempau J (2008) PENELOPE—A code system for Monte Carlo simulation of electron and photon transport, Version 2008 OECD Nuclear Energy Agency Issy-les-Moulineaux, available at http://www.nea.fr/html/science/pubs/2009/nea6416-penelope.pdf.

[14] Salvat F, Fernández-Varea JM and Sempau J (2008) PENELOPE-2008: A code system for Monte Carlo simulation of electron and photon transport Workshop Proceedings Barcelona Spain.

[15] Badal A and Sempau J (2006) A package of Linux scripts for the parallelization of Monte Carlo simulations Computer Physics Communications 175 440–50.

[16] Cullen D, Hubbell J and Kissel L (1997) EPDL97 the evaluated photon data library,'97 version, Report UCRL-50400 6(4) parts A and B Livermore, CA: Lawrence Livermore National Laboratory.

[17] Ribberfors R (1983) X-ray incoherent scattering total cross sections and energy-absorption cross sections by means of simple calculation routines Phys. Rev. A 27 3061–70.

[18] Baró J, Roteta M, Fernández-Varea JM and Salvat F (1994) Analytical cross sections for Monte Carlo simulation of photon transport Radiat. Phys. Chem. 44 531–52.

[19] Berger MJ (1963) Monte Carlo calculation of the penetration and diffusion of fast charged particles Methods in Computational Physics 1 eds.Alder BFernbach S and Rotenberg M (Academic Press, New York) pp. 135–215.

[20] Reimer L and Krefting ER (1976) The effect of scattering models on the results of Monte Carlo calculations National Bureau of Standards Special Publication 460(US Government Printing Office, Washington DC) 45–60.

[21] Andreo P and Brahme A (1984) Restricted energy-loss straggling and multiple scattering of electrons in mixed Monte Carlo procedures Rad. Res. 100 16–29.

[22] Seltzer SM and Berger MJ (1985) Bremsstrahlung spectra from electron interactions with screened atomic nuclei and orbital electrons Nucl. Instrum. Meth.B 12 95–134.

[23] Seltzer SM and Berger MJ (1986) Bremsstrahlung energy spectra from electrons with kinetic energy 1 keV–10 GeV incident on screened nuclei and orbital electrons of neutral atoms with Z=1–100 At Nucl. Data Tables 35 345–418.

[24] National Nuclear Data Center (NNDC), Brookhaven National Laboratory NUDAT2.0. Electronic Version available online at NNDC: http://www.nndc.bnl.gov/nudat2/, 2005.

[25] Chesta MA, Plievelic TS and Mainardi RT (1998) Characteristic X-rays Induced by Electrons and Positrons from b-emitting Radioisotopes, Nucl. Inst. & Methods in Phys. Res. B, 145(3) 459-68.

[26] Chesta MA, Plievelic TS and Mainardi RT (2002) A Multi-propose X-Ray Source of Tunnable Energy, Nucl. Inst. & Methods in Phys. Res. B, 187 259-63.

[27] Johns H E and Cunningham J R (1983) The physics of radiology Fourth edition Charles C Thomas Publisher Illinois 796 p.

[28] Wang R and Li XA (2002) Dose characterization in the near-source region for two high dose rate brachytherapy sources Med. Phys. 29(8)1678–86.

[29] Pérez-Calatayud J, Granero D and Ballester F (2004) Phantom size in brachytherapy source dosimetric studies Med. Phys. 31(7) 2075-81.